




A facile synthesis of Zn-doped TiO₂ nanostructures for enhanced photocatalytic performance

K. Santhi¹, S. Ponnusamy^{1,*} , S. Harish^{1,*}, and M. Navaneethan^{1,2}

¹Functional Materials and Energy Devices Laboratory, Department of Physics and Nanotechnology, SRM Institute of Science and Technology, Kattankulathur, Chennai, Tamil Nadu 603203, India

²Nanotechnology Research Center (NRC), Faculty of Engineering and Technology, SRM Institute of Science and Technology, Chennai, Tamil Nadu 603203, India

Received: 25 July 2021

Accepted: 15 February 2022

Published online:

8 March 2022

© The Author(s), under exclusive licence to Springer Science+Business Media, LLC, part of Springer Nature 2022

ABSTRACT

In recent years, environmental pollution has been considered a great concern. The environmental pollution is cleaned by filtration, ozonation, adsorption, and electrochemical reaction techniques but they cannot completely degrade the organic pollutants and these techniques are also expensive. Zn-doped TiO₂ nanoparticles were synthesized by the hydrothermal method and the photocatalytic degradation mechanism of methylene blue (MB) dye under visible light irradiation was performed. The catalyst was characterized by transmission electron microscopy (TEM), X-ray diffraction, Raman spectra, UV–Visible reflectance spectra, and X-ray photoelectron spectroscopy. The XRD and Raman results indicated that doping Zn into TiO₂ nanoparticles could exhibit the anatase phase. FESEM and TEM reveal the formation of mesoporous spherical nanoparticles. After doping absorption wavelength extended in the visible region, which is confirmed from optical spectra. The highest photocatalytic degradation rate was achieved 94% in 30 min under visible light and also fitted a pseudo-first-order equation. Zn-doped TiO₂ nanoparticles were found to be promising materials for the photocatalytic decomposition of MB under visible light.

1 Introduction

In recent years, environmental pollution from the wastewater generated by textiles, industries, domestic waste, sewage waste, etc. has been considered a great concern. It is cleaned by filtration, ozonation, adsorption, and electrochemical reaction techniques. The degradation of organic pollutants is difficult, and it is an expensive process [1]. However, the best and

the cheapest method is photodegradation. Mostly nanostructured wide-band semiconductors like ZnO, TiO₂, CuO, SnO₂, and WO₃ are apt materials for photodegradation of organic pollutants under UV, Visible, and Solar light [2]. Among these, TiO₂ is the best photocatalyst due to its high photoactivity, high quantum efficiency, chemical, and physical stability, less toxic, and low cost [3, 4]. TiO₂ has three different phases, such as anatase, rutile, and brookite phase. It

Address correspondence to E-mail: suruponnus@gmail.com; aravindharri@gmail.com

is found that the anatase phase has the best photocatalytic activity. However, a major drawback of TiO_2 is that it has a wide bandgap (3.2 eV). The TiO_2 requires UV irradiation and as solar light contains a very less percentage of UV light (4–5%), it is necessary to develop a photocatalyst that should be activated by visible light. This could be done by doping with metal and non-metals [5]. Doping with transition metals, like Fe^{2+} , Mn^{2+} , Cu^{2+} , and Zn^{2+} , is the most powerful way to improve the photocatalytic activity of titania. Among all the transition metal ions Zn^{2+} is the best dopant for doping due to its ionic radii [6]. Zn-doped TiO_2 is being synthesized by sol–gel [7], co-precipitation [8], the hydrothermal method [9], and solid-phase reaction [10]. The hydrothermal reaction is the suitable method for the synthesis of transition metal-doped titania, and it has some advantages when compared to other conventional methods, like uniform particle size, different morphologies, good homogeneity, and porosity [11, 12]. The various reports have demonstrated different catalysts for the degradation of MB dye, such as Nb-doped TiO_2 [13], CuO/ZnO nanocomposites [14] palladium-doped TiO_2 [15], silver-doped TiO_2 [16], (Fe, N, Sb, Ce, S, Zr, C)-doped TiO_2 [17], and Cu-doped TiO_2/ZnO [18]. Among these, Zn-doped TiO_2 is the best candidate for photocatalysis due to its inexpensive, non-toxic, wide bandgap, high stability, and easy availability. Benjwal et al. reported that Zn-doped TiO_2 nanotube synthesized by anodization method showed 90% degradation efficiency of MB under the visible light [19]. Seo et al. reported that photocatalytic activity is increased with the increasing amount of Zn particles. Especially, in the case of $\text{TiO}_2:\text{Zn}$ (1:0.1 mmol) mixture photocatalyst provide 2 times higher photocatalytic activity compared with the commercially available TiO_2 photocatalyst [20]. Jiang et al. have prepared Zn-doped TiO_2 by one-step hydrothermal decomposition method. According to the authors, the degradation efficiency of RhB was achieved 98.7% in 60 min, under the irradiation of visible light [21]. Rajaraman et al. have reported that Zn-doped TiO_2 was prepared by solvothermal method, and it showed complete degradation of MB within 3 h of solar light illumination [22]. Li et al. have reported that Bi–Zn-co-doped TiO_2 catalysts were prepared by the solvothermal route and it showed that Zn acts as a mediator for internal charge transfer. The degradation efficiency of toluene was achieved 93% in 200 min under visible light [23]. Gupta et al. have reported that

ZnO: TiO_2 catalysts were prepared by solid-state reaction method and 92% of quinoline degradation was achieved in 240 min under UV light [24]. Zhang et al. reported Potassium bichromate was degraded 40% in 150 min under Fluorescent lamp [25]. Zn-doped TiO_2 was prepared by Nguyen et al. [7] under sol–gel method. According to author 91.4% methylene blue (MB) degradation was achieved in 240 min under black-light blue lamps. Therefore, systematic investigations on tuning the bandgap of TiO_2 by preparing Zn-doped TiO_2 nanocomposites to enhance the photocatalytic activity is essential. In this article, Zn-doped TiO_2 nanoparticles were synthesized by the hydrothermal method. The structural, optical, morphological behavior, and the photocatalytic activities of as-prepared Zn- TiO_2 have been studied against MB under the visible light irradiation and the results are reported here.

2 Experimental procedure

2.1 Synthesis of Zn-doped TiO_2

For synthesis of Zn-doped TiO_2 nanoparticles, the precursors, titanium tetraisopropoxide [$\text{Ti}(\text{OCH}(\text{CH}_3)_2)_4$, 98%], Zinc acetate dihydrate [$\text{Zn}(\text{CH}_3\text{CO}_2)_2 \cdot 2\text{H}_2\text{O}$, 98%], Ammonia [NH_3 , 98%], Ethanol [$\text{C}_2\text{H}_5\text{OH}$, 98%], and MB [$\text{C}_{16}\text{H}_{18}\text{ClN}_3\text{S}$, 99%] were purchased from Merck and were used without further purification. In typical synthesis $\text{Ti}_{(1-x)}\text{Zn}_x\text{O}_2$ with $x = 0.1, 0.3, \text{ and } 0.5$ were prepared by the hydrothermal method. Titanium tetraisopropoxide and zinc acetate dihydrate were used as the precursors of Ti and Zn, ammonia as a surfactant, and ethanol as a solvent. The synthesis procedure was carried out as follows. 5 mL of titanium tetraisopropoxide was dissolved in 50 mL of ethanol. Zinc solution was prepared using zinc acetate at 0.1, 0.3, and 0.5 wt% in 50 mL of DI water. After complete dissolution both the solutions were mixed. Ammonia was added to the mixture to maintain $\text{pH} = 7$ and then it was transferred to an autoclave which was heated at 180 °C for 24 h. The obtained precipitate was separated by centrifugation, washed with deionized water and ethanol several times, and then dried at 80 °C for 3 h. The dried samples were annealed at 400 °C for 5 h. The resulting samples are labeled as ZT1 for 0.1% Zn, ZT2 for 0.3% Zn, and ZT3

for 0.5% Zn and are stored in an airtight container for further studies.

2.2 Characterization

The structure and phase of the synthesized samples were characterized using an X' Pert PRO (PAN analytical diffractometer using K_{α} ($\lambda = 1.5405 \times 10^{-10}$ m) radiation at a scan rate of $0.02^{\circ}/s$. The morphology was measured by FEI Quanta FEG200 Field Emission Scanning Electron Microscope (FESEM). Transmission electron microscopy (TEM) images were recorded using a JEOL JEM 2100F microscope at an accelerating voltage of 200 kV. Functional group analysis was carried out by Bruker IFS 88 Fourier Transform Infrared (FTIR) spectrometer equipped with an MCT cryodetector. Optical absorption studies were done by Shimadzu UV-2600 spectrophotometer. X-ray photoelectron spectra (XPS) were measured by Shimadzu ESCA 3100.

2.3 Photocatalytic measurement

The photocatalytic activities of the Zn-doped TiO_2 nanoparticles were tested against MB dye in an aqueous solution. The degradation experiment was carried out by employing an immersion-type photoreactor constructed by a double-layer quartz tube container. The photocatalytic activity was carried out using a 150 W (Heber Scientific Suppliers) tungsten lamp of 400 nm wavelength and the irradiation intensity measured by lux meter was 23,000 lux. The aqua MB dye solution (100 mL; 3 ppm) was prepared. The absorption spectrum recorded using a UV-Visible spectrometer showed maximum absorption intensity at 664 nm. Then, 10 mg of synthesized sample was added to the MB dye solution and the solution was continuously stirred for 10 min in dark conditions to analyze adsorption and desorption equilibrium between the catalyst and MB dye. The stable aqueous dye solution was exposed to visible light irradiation for 10 min and at every 10-min interval, the UV absorption spectra were recorded and continued for a total period of 30 min at the end of the cycle, the solution was centrifuged to separate TiO_2 particles. The photodegradation percentage of MB is calculated from the following Eq. (1) [26, 27].

$$D(\%) = \left[\frac{1 - C_t}{C_0} \right] \times 100, \quad (1)$$

where C_0 is the initial concentration of the dye solution and C_t is the concentration of the dye solution at every 10-min interval during the photocatalytic reaction.

3 Results and discussion

The phase purity and crystal structure of the Zn-doped TiO_2 nanoparticles (ZT1, ZT2, ZT3) were determined by XRD as shown in Fig. 1a. The diffraction peaks are observed at 25.22° , 37.89° , 47.92° , 53.98° , 54.99° , 62.67° , 68.91° , 70.22° , and 75.05° for ZT3 which corresponds to (1 0 1), (0 0 4), (2 0 0), (1 0 5), (2 1 1), (2 0 4), (1 1 6), (2 2 0), and (2 1 5) lattice planes of the tetragonal structure of anatase phase TiO_2 . These values are well matched with JCPDS Card No. (21-1272) [28]. It is observed that the diffraction angle of ZT3 slightly shifts to the lower angle (less than 0.09 degree) when compared to ZT1 [29]. Figure 1b is the extended view of XRD. It shows that the diffraction peak position slightly shifts to a lower angle with increasing Zn concentration. When the concentration of Zn increases, the particle size increases due to the formation of ZnO, and the ionic radius of Zn^{2+} (0.072 nm) is larger than that of Ti^{4+} (0.061 nm), [30, 31]. The interplanar distance increases from 0.348 to 0.350 nm which is calculated from Bragg's equation. This confirms the size increases after Zn doping, which reveals the incorporation of dopants in the host crystal lattice [32].

The crystal phases of Zn-doped TiO_2 nanoparticles can be identified by Raman spectroscopy. Raman spectra of Zn-doped TiO_2 nanoparticles are shown in Fig. 2. The peak at 143.2 cm^{-1} (sharp and strong), 197.4 cm^{-1} (very weak), and 637 cm^{-1} (weak) corresponds to the E_g mode of symmetric stretching vibrations of O–Ti–O [33]. The other peaks at 396.7 cm^{-1} were assigned to B_{1g} mode due to the symmetric bending vibrations and 515 cm^{-1} assigned to A_{1g} mode due to the anti-symmetric bending vibrations [34, 35]. As Zn content increases, the intensity of Raman peak decreases as well as a slight shift is observed in B_{1g} mode (from 396.7 to 399 cm^{-1}) of TiO_2 . This confirms the presence of Zn atom in the TiO_2 lattice, which leads to the formation of a new bond Zn–O–Ti in the lattice [36, 37]. This shift is responsible for the generation of defects like oxygen vacancies in the host lattice and an increase in

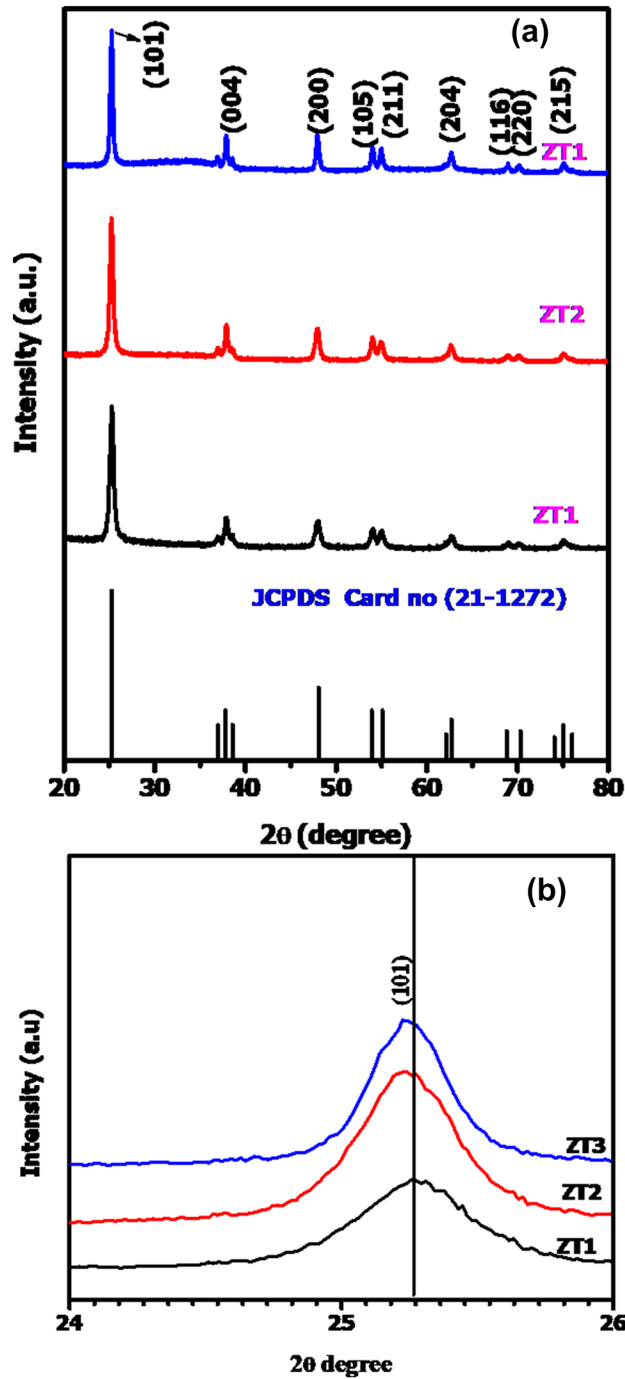


Fig. 1 a XRD pattern of Zn-doped TiO₂ samples and b extended view of XRD

crystallite size. A similar trend in XRD confirms the presence of Zn atom in the TiO₂ lattice.

The morphology of the Zn-doped TiO₂ nanoparticles was predicted by FESEM analysis. The obtained micrographs are presented in Fig. 3. All the samples are globular, small aggregate mesoporous nanoparticles

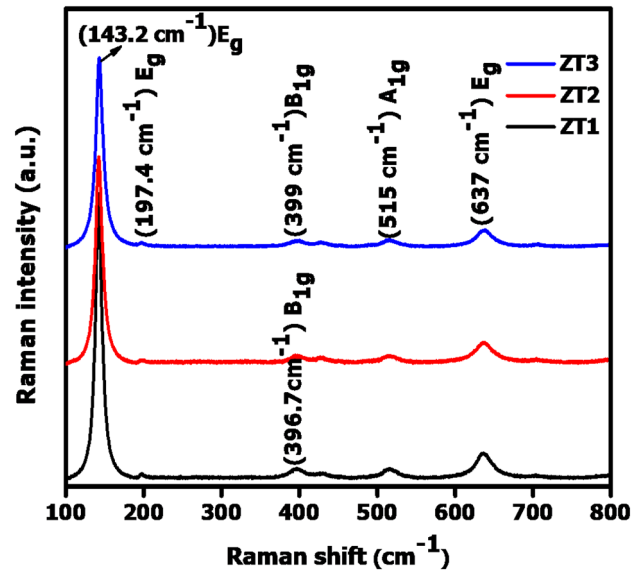


Fig. 2 Raman spectra of Zn-doped TiO₂ nanoparticles

grown one on the other as presented in Fig. 3(1(a)) and (2(a)). The particle size as measured through image] analysis is found to be in the range of 10–25 nm [38, 39]. When the concentration of Zn increases the TiO₂ surface is densely surrounded by ZnO nanoparticles due to this cauliflower-like structure formed as shown in Fig. 3(3(a)). TEM images of the samples reveal that the particles are agglomerated and have a size distribution around 10 nm–20 nm [40] as shown in Fig. 3(1(b))–3(b)). From the HRTEM images [Fig. 3(1(c)) to (3(c))], it is apparent that the particle are non-uniform and highly crystalline. The uniform fringes with a lattice spacing of 0.35 nm corresponding to (101) anatase phase are observed. Many researchers reported different morphologies, like nanorods, nanotube, and nanosphere. Among these the catalyst with spherical nature can provide large surface area, ample transportation, penetration of light waves deep into the catalyst, and more reactive sites induced during the photocatalytic reaction, which can enhance the photocatalytic degradation process [41, 42]. EDAX was performed using FESEM. EDAX spectra of Zn-doped TiO₂ are represented in Fig. 4a–c. It demonstrates the presence of Ti and Zn and inserted table shows the approximate weight percentage of prepared samples.

FTIR was used to identify the functional groups and chemical bonding in TiO₂ and ZnO nanoparticles in the wavenumber range of 400 cm⁻¹ to 4000 cm⁻¹. Figure 5 shows the FTIR spectra of Zn-doped TiO₂ nanostructures. The absorption band around 3651 cm⁻¹ which is assigned to the stretching vibration

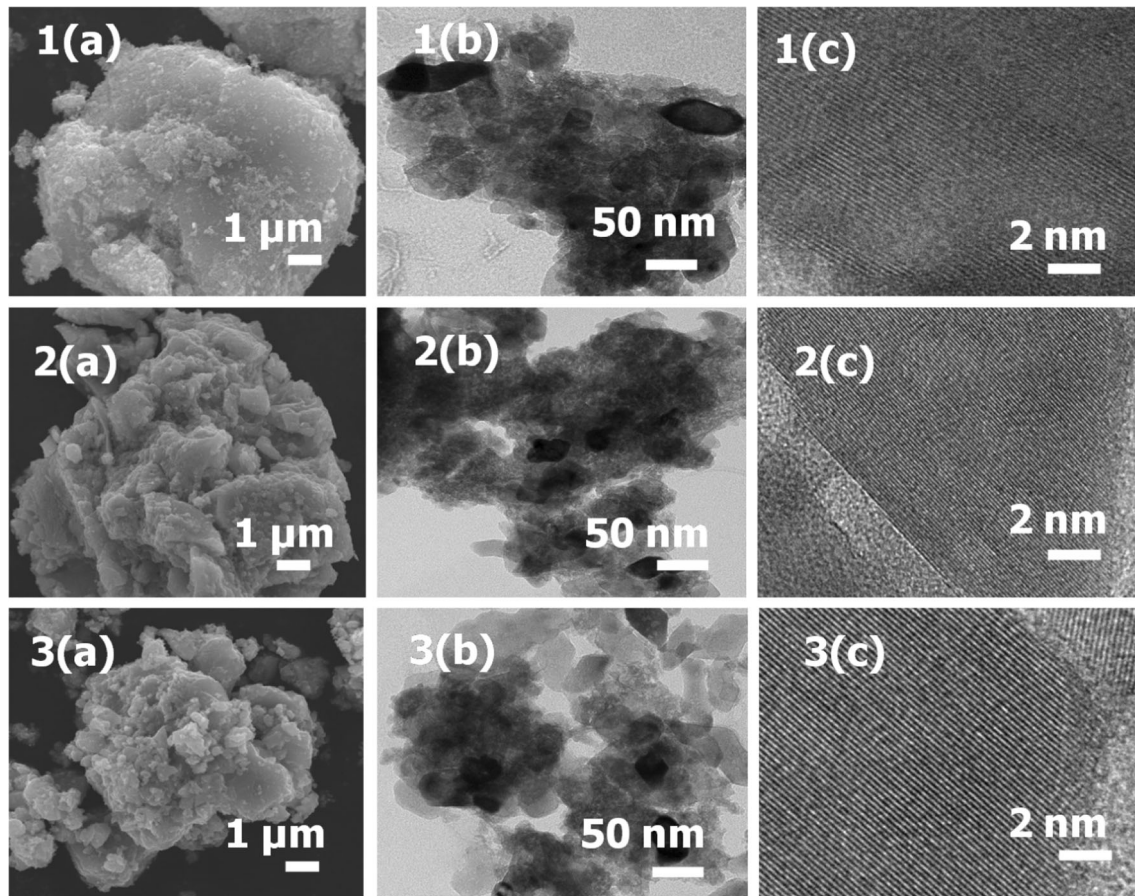


Fig. 3 FESEM, TEM, and HRTEM images of ZT1 [1(a), (b), and (c)], ZT2 [2(a), (b), and (c)], and ZT3 [3(a), (b), and (c)]

of the hydroxyl group ($-\text{OH}$) and 1635 cm^{-1} is assigned to the bending mode of hydroxyl group ($-\text{OH}$) vibrations [43, 44]. The absorption band at 2339 cm^{-1} can be assigned to anti-symmetric stretching vibrations of the CO_2 band [45]. The peak at 667 cm^{-1} is assigned to vibration modes of metal–oxygen bonds like $\text{Zn}-\text{O}$ and the small peak at 458 cm^{-1} corresponds to $\text{Ti}-\text{O}-\text{Ti}$ bonds [46, 47]. These results confirm that Zn is incorporated into the TiO_2 structure. The peak at 667 cm^{-1} is assigned to vibration modes of metal–oxygen bonds like $\text{Ti}-\text{O}-\text{Ti}$ and corresponds to $\text{Zn}-\text{O}$ bonds.

The optical absorption of the samples was studied by UV–Vis diffuse reflectance spectra as shown in Fig. 6a. From Table 1, many researchers reported [7, 16, 24, 53, 60, 62–64] better degradation performance under UV. Tariq et al. [48] reported that Zn-doped TiO_2 exhibited the highest Transmittance value in the visible spectrum (400–800 nm). The fundamental absorption edge was found to be located at 350 nm for pure TiO_2 , which was noticed to

have a redshift to 396 nm upon Zn doping by 0.1 mol%, thus indicating a reduction in the bandgap energy (E_g) due to the formation of intermediate donor levels below the conduction band (CB).

The sample ZT1 displayed an absorption peak at 396 nm. Moreover, the absorption peak shifted to a higher wavelength of 412 nm for ZT2 and 415 nm for ZT3. The observed peak shift in UV spectra corresponds to the redshift. The redshift implies that the introduction of a new impurity level in between the CB and valance band (VB) of TiO_2 by doping of Zn [49]. When the concentration of Zn increases, the absorption edge shifted to the visible region. This may be assigned to the Zn which can dope into the surface of TiO_2 particles and decrease the bandgap [50]. The bandgap of the samples is calculated using the Tauc's plot equation given by

$$(\alpha h\nu) = A(h\nu - E_g)^n, \quad (2)$$

where α , ν , A , and E_g are the absorption coefficient, frequency, proportionality constant, and bandgap

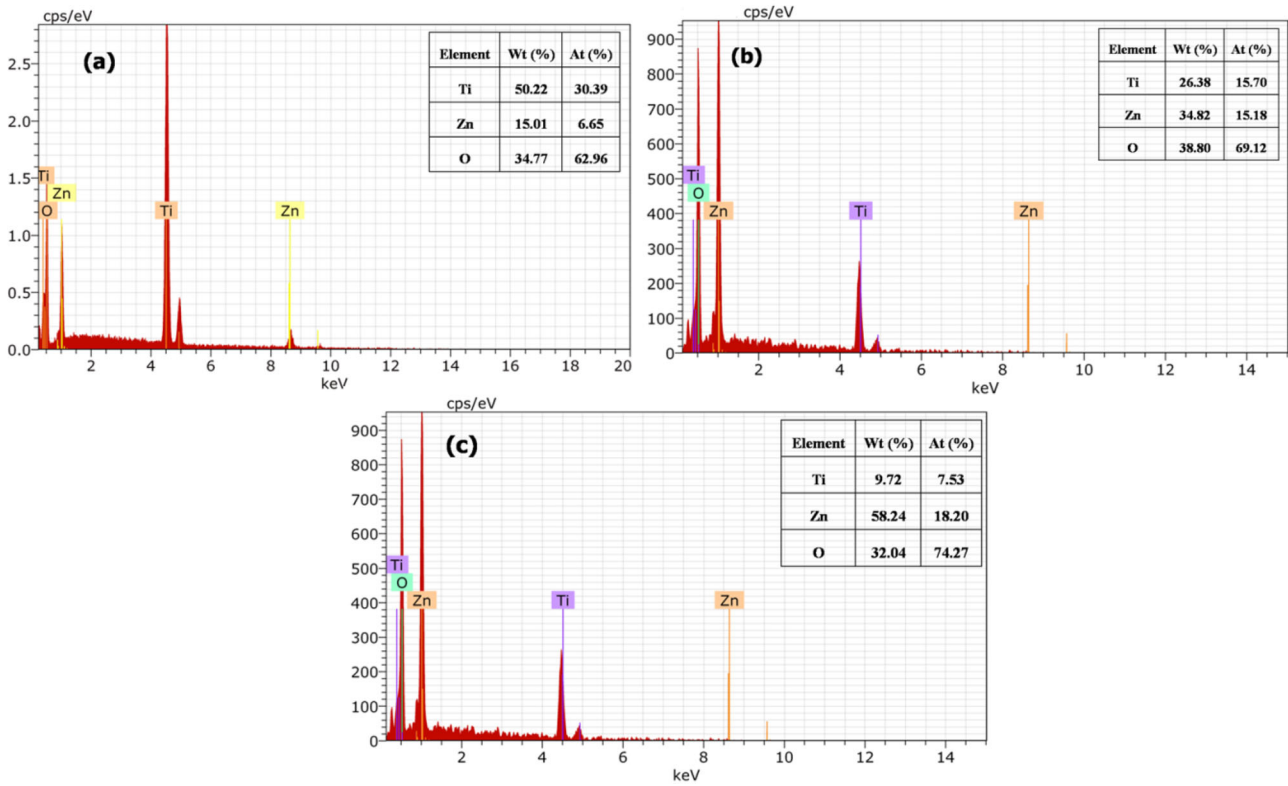


Fig. 4 EDAX analysis of Zn-doped TiO₂: a ZT1, b ZT2, and c ZT3

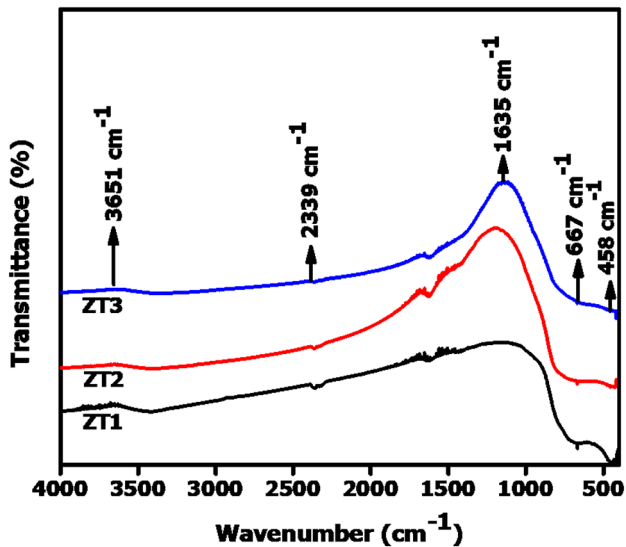


Fig. 5 FTIR spectra of Zn-doped TiO₂

energy, respectively. In above equation $n = 2$ is a constant for direct transition [51]. The bandgap values of samples ZT1, ZT2, and ZT3 are 3.13 eV, 3.08 eV, and 2.98 eV as Zn content increases from 0.1 to 0.5 wt% as shown in Fig. 6b. The obtained bandgap values of doped TiO₂ nanostructures of the

present work suggest the enhancement in the photocatalytic activity.

XPS was used to investigate the surface composition and chemical states of Zn-doped TiO₂ nanoparticles. Figure 7a shows that Ti 2p of Zn-doped TiO₂ has two peaks, such as Ti 2p_{3/2} and Ti 2p_{1/2}. Both of the peaks can be observed at 458 eV and 464 eV attributing to Ti⁴⁺ [52, 53]. These values are much lower in binding energy compared to other reported values of pure TiO₂, this implies that Zn is present in the TiO₂ lattice. Similar results were reported by Benjwal et al. [19]. Figure 7b shows the state of the Zn-doped TiO₂ sample. The Zn 2p was divided into two states such as Zn 2p_{3/2} and Zn 2p_{1/2} due to spin-coupled states. The peak at 1022.1 eV and 1045.4 eV corresponds to Zn 2p_{3/2} and Zn 2p_{1/2}, respectively. This confirms the presence of Zn²⁺ in the prepared sample [54]. The peak was shifted toward higher binding energies, and this indicates the presence of Zn species interstitially on the host lattice [55]. Figure 8a–c shows the core-level spectra of the O1s, and the peaks at 529.6 eV (ZT1), 529.6 eV (ZT2), and 529.7 eV (ZT3) corresponds to lattice oxygen (OL) of TiO₂ and 530.1 eV (ZT1), 530.2 eV (ZT2), and

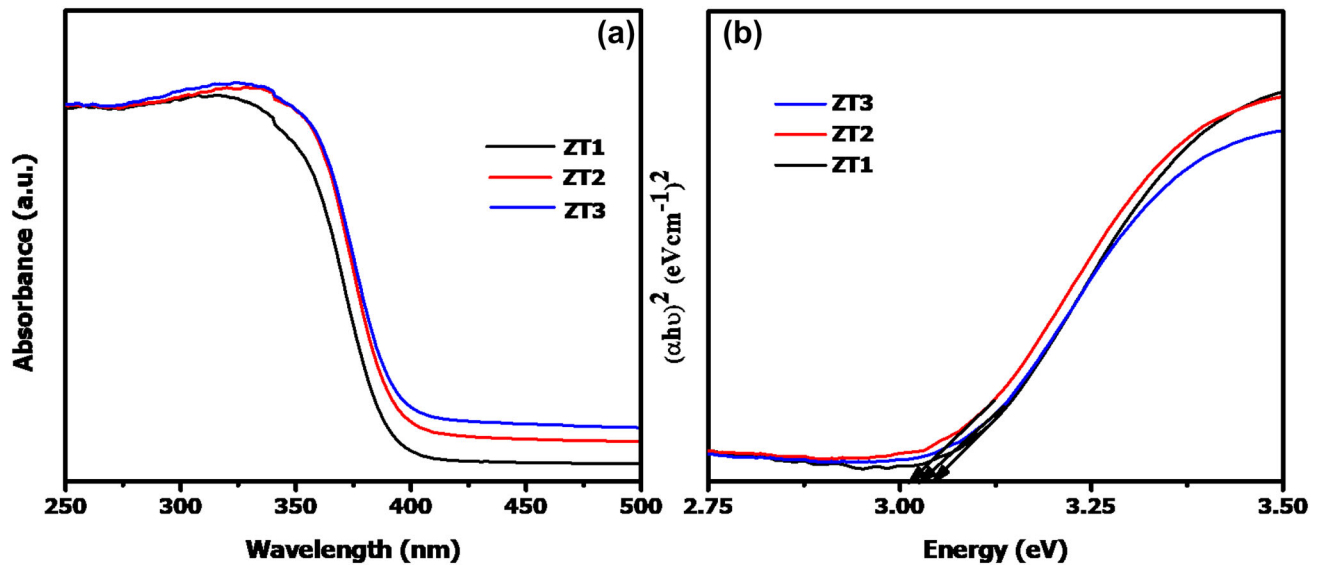


Fig. 6 **a** UV–Vis diffuse reflectance spectra Zn-doped TiO₂ nanoparticles and **b** Tauc plot of Zn-doped TiO₂ nanoparticles

530.4 eV (ZT3) is assigned to the binding oxygen (OB) of ZnO. The O1s peak of ZT3 was slightly shifted to higher binding energy compared to ZT1. This implies that the oxygen atoms increase on the surface of the TiO₂. It indicates that sample ZT3 possesses a more oxygen defect state compared to ZT1. Hence, sample ZT3 has more oxygen vacancies which enhance the photocatalytic activity [56]

3.1 Photocatalytic activity of Zn-doped TiO₂

Methylene blue was considered as a model dye to evaluate the photocatalytic activity of the photocatalysts under visible light irradiation and the results are shown in Fig. 9. Three ppm of aqueous MB was prepared by 100 mL using deionized water. The dye solution with the catalyst was stirred in the dark for 10 min until adsorption–desorption equilibrium is achieved. To achieve an absorption–desorption equilibrium state the solution need to be kept in the dark before light irradiation. This is then commonly analyzed in terms of the Langmuir model for absorption and subsequently, in terms of the Langmuir–Hinshelwood model from the point of view of kinetics. Although in many cases the absorption–desorption equilibrium is achieved very rapidly, some cases may take longer, thus the reason for relatively long periods is being left in fundamental studies. No significant decrease in the concentration of the dye was observed after 10 min for all the

samples. Initially, degradation of MB in presence of 10 mg/100 mL of catalyst was tested without light for 30 min. For all the samples, the decrease in absorbance was only 13%–15% in absence of light. The decrease in absorbance can be attributed to the adsorption of dye on the catalyst surface and not because of the photodegradation activity of the catalyst. Figure 9a–c shows time-dependent UV–Visible absorption spectra of the MB solution in the presence of Zn-doped TiO₂. The dominant absorption of MB is registered at 664 nm. After 10 min absorption is rapidly decreased to 640 nm due to the hypsochromic effect. The highest degradation efficiency is 94%. Different contents of Zn on the photodegradation of MB under visible light are shown in Fig. 9d. When Zn dopant increases from 0.1 to 0.5%, its photocatalytic activity increases. The degradation percentage is calculated to be 93% for ZT1, 79.5% for ZT2, and 94% for ZT3, respectively. The comparison was made between the photocatalytic decomposition performed in this work and other reported work as shown in Table 1.

Photocatalytic activity mainly depends on the recombination rate of photogenerated electrons and holes produced in the subject of photodegradation of MB under visible light. Zn and TiO₂ are both wide bandgap semiconductors. Even though the bandgap of Zn (3.37 eV) is larger than TiO₂ (3.2 eV) the Fermi level of TiO₂ is lower than that of ZnO [57]. It means that the photogenerated electrons readily transfer from ZnO to TiO₂ due to the sub-energy level lying

Table 1 Comparison on the photocatalytic performances of Zn-doped TiO₂ nanostructures in this research with that of those reported in various literatures

S.no	Year	Author	Material	Morphology	Light source	Dye	Irradiation time (min)	Degradation percentage (%)
1	2011	Nguyen et al. [7]	Zn-doped TiO ₂	Spherical	Black-light blue lamps	Methylene blue	240	91.4
2	2017	Khaki et al. [60]	Cu-doped TiO ₂ /ZnO	Nanorod	Fluorescent lamp	Methylene blue	150	76.8
3	2016	Chen et al. [53]	ZnO/TiO ₂	Nanofiber	UV light	Methyl orange Rhodamine B	150 16	87.43 92.57
4	2012	Zhang et al. [61]	TiO ₂ /ZnO	Nanofiber	Mercury light	Methyl orange	40	85
5	2013	Pant et al. [62]	TiO ₂ /ZnO	Nanoflower	UV light	4-Nitrophenol Methylene blue	40 120	95 68
6	2012	Pan et al. [63]	ZnO Nanoflower containing TiO ₂	Nanoflower	UV light	Methylene blue	180	69.7
7	2019	Zhang et al. [25]	transition metal (Cu, Fe, Zn)-doped TiO ₂	Nanoclusters	Fluorescent lamp	Potassium bichromate	150	40
8	2007	Huimin et al. [64]	Zn-doped TiO ₂	Nanotube	Visible light	Pentachlorophenol	120	18.4
9	2020	Gupta et al. [24]	ZnO:TiO ₂ mixed oxide	Spherical	UV light UV light	Pentachlorophenol quinoline	120 240	73.5 92
10	2018	Nguyen et al. [15]	Palladium-doped TiO ₂	Spherical	UV light	Methylene blue	120	99.4
11	2012	Nainani et al. [16]	Silver-doped TiO ₂	Spherical	UV light	Methyl orange Methyl orange	180	91.5
12	2014	Bhosale et al. [17]	Doped TiO ₂	Spherical	Solar light	Methylene blue	60	93.1 91.3 85 80 37 80 98.7
13	2018	Khaki et al. [18]	Cu-doped TiO ₂ /ZnO	Nanoparticle	Visible light	Methylene blue Methyl orange	120	73.2 85.5
14		Present work	Zn-doped TiO₂	Spherical	Visible light	Methylene blue	30	94

C-TiO₂ corresponds to carbon decorated TiO₂ nanostructure and Zn-TiO₂ is present work reported in this manuscript are given in bold

very close to the CB of TiO₂, and the photogenerated electrons at the CB can be transferred to the doping energy level. Thus, the dopant acts as efficient electron traps, which promote the separation of photo-generated electrons and holes and enhance the

photocatalytic activity. Figure 9e shows the photodegradation of MB solution for different photocatalysts. A quantitative relationship of the enhanced photocatalytic activity was studied using the Langmuir–Hinshelwood kinetics model. Figure 9f shows

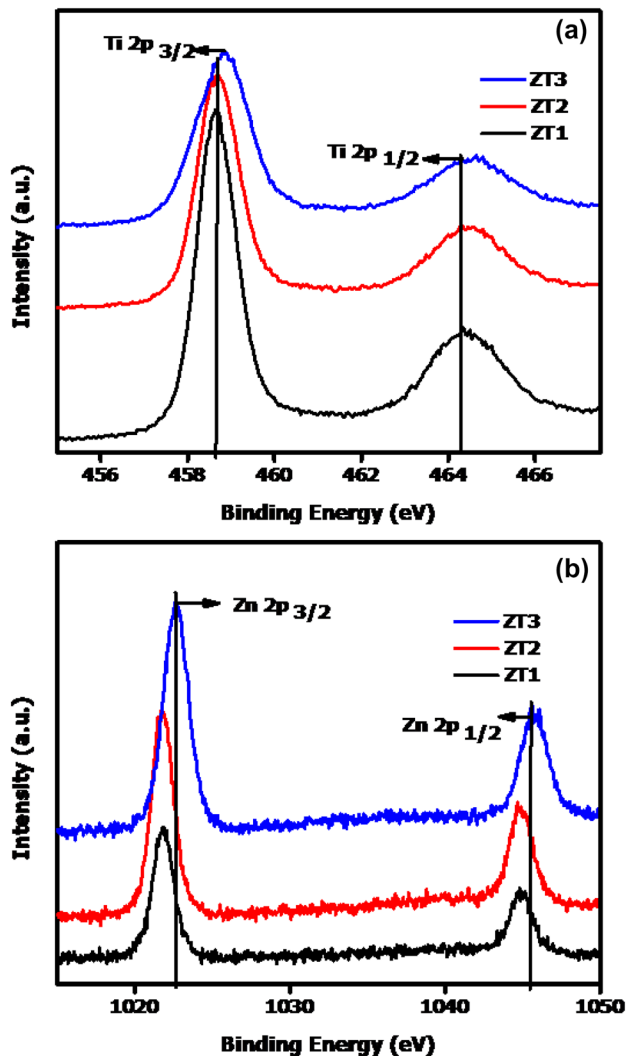


Fig. 7 XPS core-level spectra of Zn-doped TiO₂ for a Ti 2p and b Zn 2p

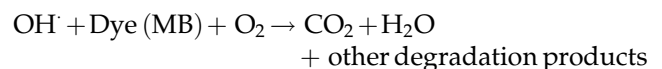
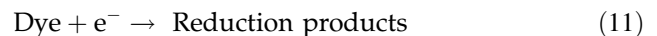
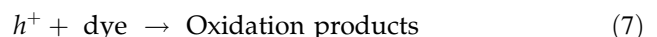
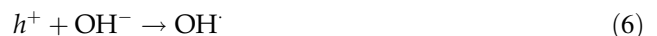
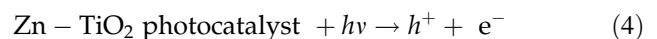
the kinetic curve of photocatalytic degradation of MB with different catalysts. The degradation of MB under visible light obeyed the pseudo-first-order reaction kinetics as follows,

$$\ln \left[\frac{C_0}{C_t} \right] = K_{\text{obs}} t, \quad (3)$$

where C_0 is the initial concentration of the dye solution, C_t is the concentration of the dye solution at every 10 min, and K_{obs} is the apparent rate constant. The values for the degradation rate constant are shown in Table 2. The higher rate constant of about 0.07625 min^{-1} at ZT3 against MB dye solution is due to the presence of relatively higher OH^- ions which readily react with holes to form free radicals [51].

3.2 The plausible photocatalytic mechanism of Zn-doped TiO₂ nanoparticles

The Plausible photocatalytic mechanism of Zn-doped TiO₂ nanoparticles toward the degradation of MB under visible light is illustrated in Fig. 10. The Zn-doped TiO₂ sample is exposed to visible light electron transfer from VB to CB, leaving a hole in the VB at both the catalysts. Electron transfer from the CB of ZnO to the CB of TiO₂ and holes transfer from the VB of TiO₂ to the VB of ZnO. Moreover, the electron may react with dissolved oxygen forming superoxide radicals (O_2^-). The hole in the VB reacts with a water molecule to produce hydroxyl radicals (OH^\cdot). After doping sub-bands are formed into the forbidden band of TiO₂ lattice, as a result the bandgap energy decreased. When increasing the content of Zn photocatalytic activity increases up to optimum weight of Zn. The optimum content of Zn is the important factor for photocatalytic performance. Beyond the optimum weight, Zn acts as a recombination center where it induces the electrons/holes pair recombination, thus reducing the photocatalytic activity as shown in Fig. 10. Due to that recombination of charge carriers was suppressed and enhanced the photocatalytic efficiency [53]. The steps in the mechanism of the photocatalytic degradation equation are shown below [58].



To study the photocatalytic process under visible light, active species generated during the reaction were identified by electron and hole scavenging experiments. To detect the active species during the photocatalytic reaction, benzoic acid (BA) and the

sodium salt of ethylenediamine tetraacetate (EDTA) were introduced into the catalyst solution as scavengers, respectively, of electrons and holes. The photodegradation of MB catalyzed by ZT3 in the presence of these various scavengers under visible light illumination is shown in Fig. 11. Compared with the scavenger-free system, the dye degradation efficiency in the presence of Electron scavenger BA was 54.26%. In contrast, the reaction with the addition of hole scavenger EDTA was almost inhibited with 72.43% of MB degradation after 30 min. This may be concluded that hole (h^+) radical is the major oxidative species responsible for photooxidative conversion of MB [59]

Fig. 9 a–c for ZT1 to ZT3, time-dependent UV–Visible absorption spectra of the MB solution in the presence of Zn-doped TiO_2 . d Different contents of Zn on the photodegradation efficiency of MB under visible light. e Photodegradation of MB solution for different photocatalysts. f Kinetic curve of the different photocatalysts

3.3 Reusability

Studying the stability and reproducibility of the photocatalyst is very important. Hence, the photocatalyst was monitored by repeating the reaction procedure. At the end of each reaction, the photocatalyst was cleaned using ethanol and distilled

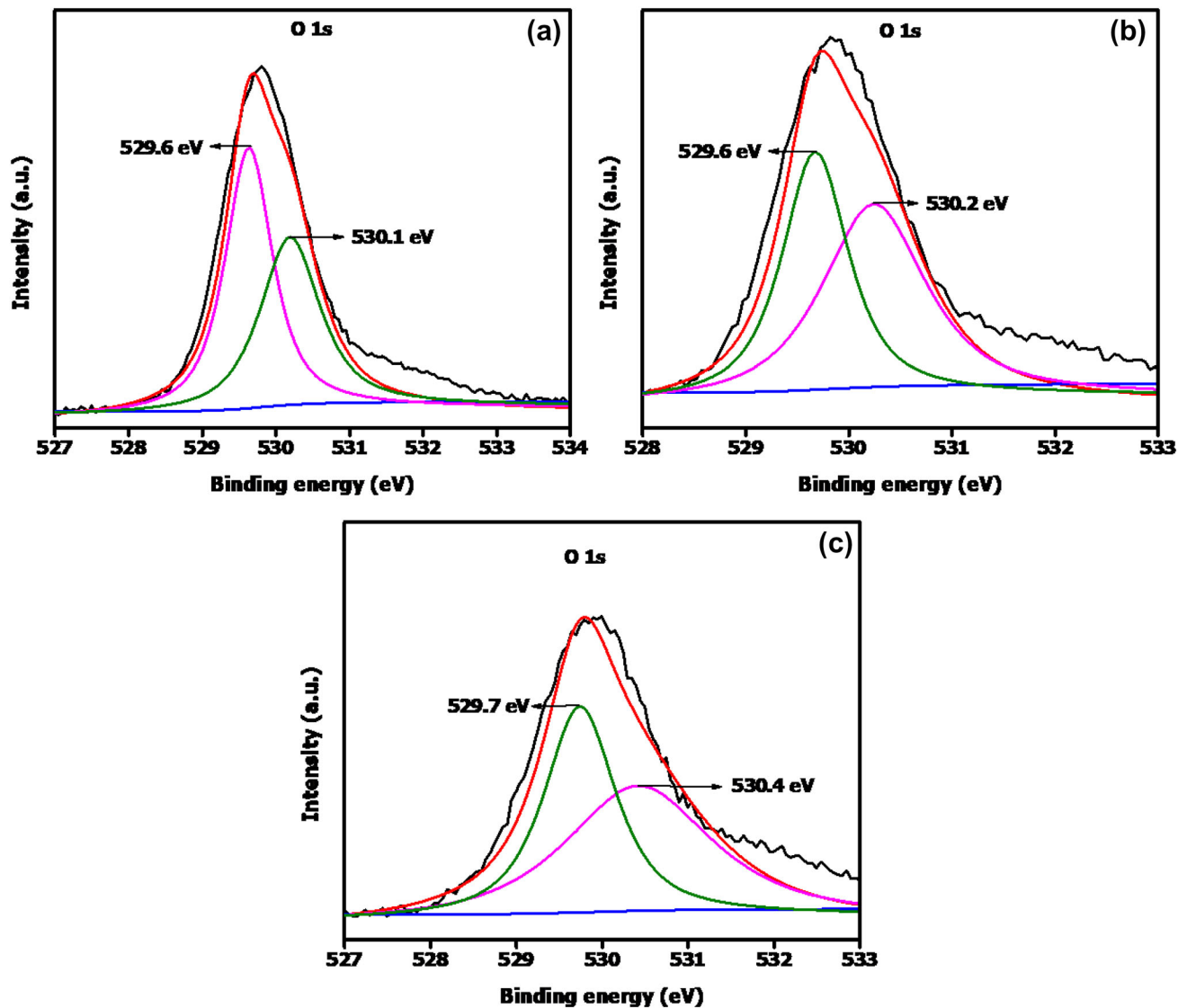


Fig. 8 XPS spectra of Zn-doped TiO_2 for O 1s: a ZT1, b ZT2, and c ZT3

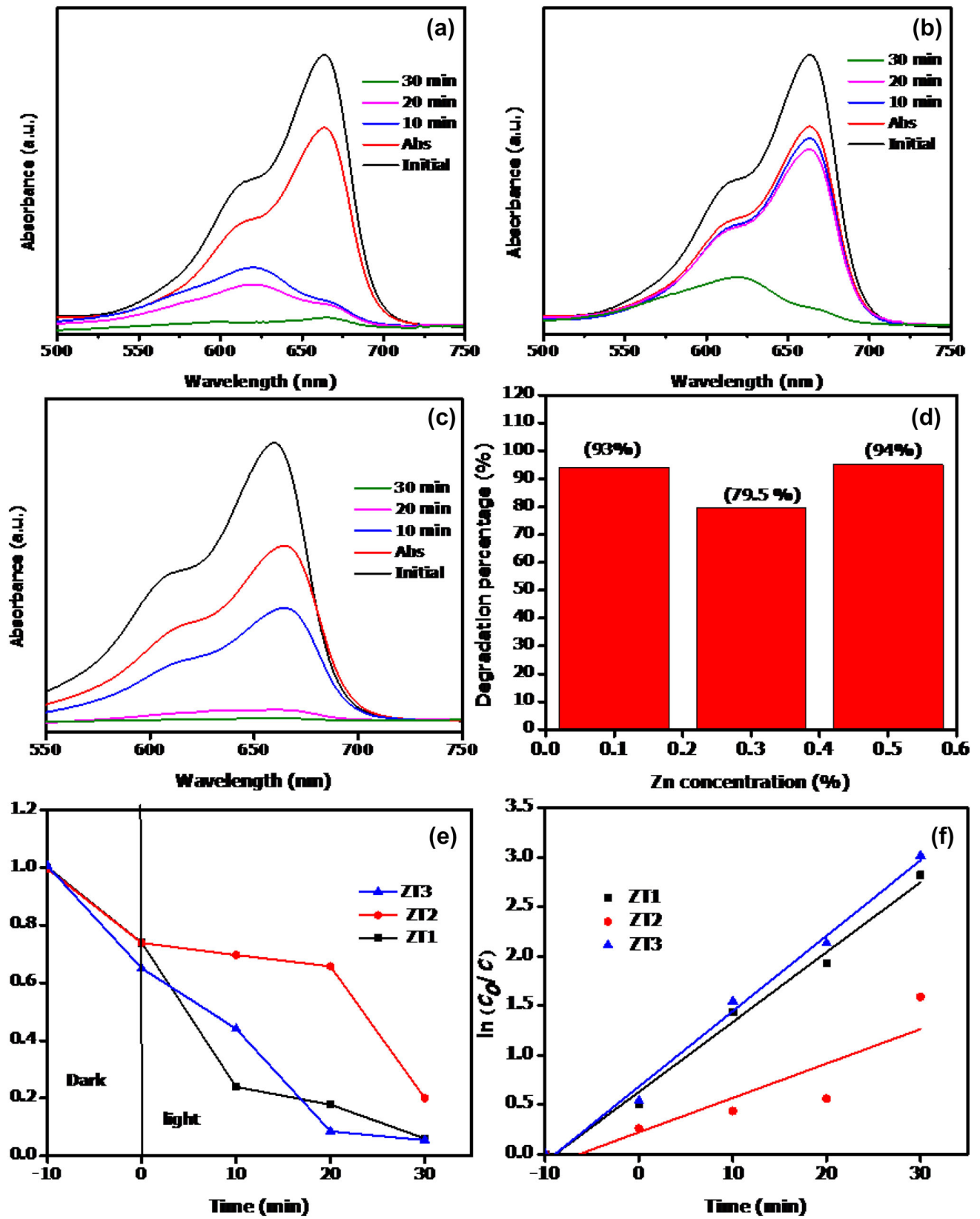


Table 2 Observed pseudo-first-order rate constants, R^2 values, maximum degradation (%), and time required for maximum degradation of Zn-doped TiO₂ nanostructures

Sample	K_{obs} (min ⁻¹)	R^2	Maximum degradation (%)	Time taken for maximum degradation (min)
ZT1	0.07066	0.9869	93	30
ZT2	0.03481	0.7596	79.5	30
ZT3	0.07625	0.9898	94	30

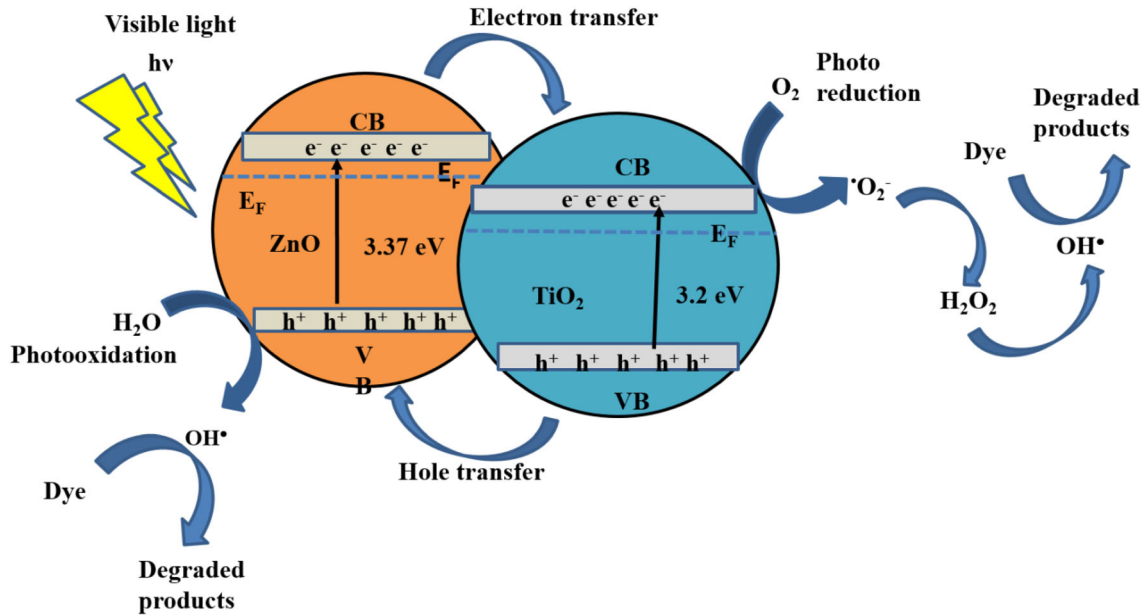


Fig. 10 Plausible mechanism of the MB degradation using the Zn-doped TiO₂ nanoparticles

water to get precipitate. Then dried in hot air oven 80 °C for 1 h to reuse for the next reaction. The degradation rate was detected at 94% for the first time, the second time slightly decreased to 92.8%, and the third time 91.3% as shown in Fig. 12. This clearly shows that ZT3 has a better stability.

4 Conclusion

Zn-doped TiO₂ nanostructures were synthesized by hydrothermal method with different Zn concentrations. XRD and Raman analyses confirm the formation of a pure anatase form of TiO₂ with a tetragonal structure. FTIR was used to identify the functional groups of metal–oxygen bonds, like Ti–O and Zn–O bonds. When the concentration of Zn increases the TiO₂ nanocrystals are densely surrounded by ZnO nanoparticles and this was confirmed by the

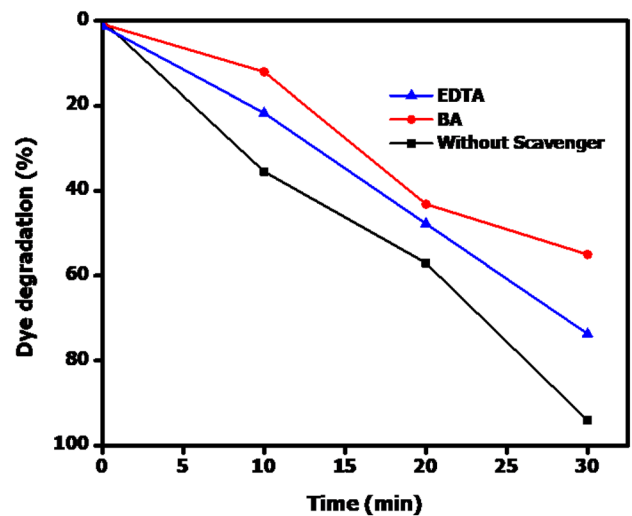


Fig. 11 Effect of MB degradation over ZT5 in the presence of various scavengers

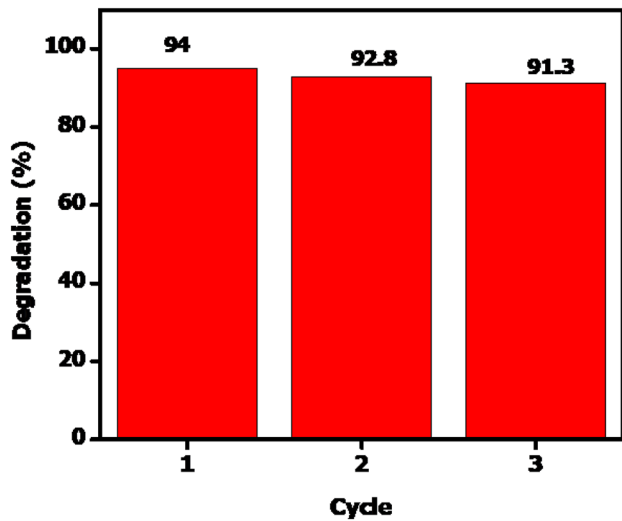


Fig. 12 Reusability of MB solution for the ZT3 sample under visible light irradiation

formation of a cauliflower-like structure from FESEM. From the optical absorption spectra, the binding energy of the synthesized samples decreased from 3.13 eV to 2.98 eV, as the Zn content increases. The shift in XPS analyses confirms the incorporation of Zn in TiO₂ lattice. Photocatalytic activity of the samples was studied and the sample ZT3 showed a higher apparent rate constant of about 0.07625 min⁻¹ and degradation efficiency value (94%) in 30 min under visible light.

Author contributions

KS contributed to conceptualization, investigation, methodology, data curation, and writing of the original draft. SP contributed to supervision, validation, formal analysis, resources, and reviewing and editing of the manuscript. SH contributed to validation, formal analysis, resources, and reviewing and editing of the manuscript. MN contributed to validation, formal analysis, and resources. All authors have read and agreed to the published version of the manuscript.

Funding

The authors have not disclosed any funding.

Data availability

My manuscript has no associated data. All data generated or analyzed during this study are included in the manuscript.

Declarations

Conflict of interest As a corresponding author I state that we don't have any conflict of interest to our research paper.

References

1. K.D. Shitole, R.K. Nainani, P. Thakur, Preparation, characterisation and photocatalytic applications of TiO₂-MWCNTs composite. *Def. Sci. J.* **63**(4), 435–441 (2013)
2. Y. Han, H.S. Kim, H. Kim, Relationship between synthesis conditions and photocatalytic activity of nanocrystalline TiO₂. *J. Nanomater.* (2012). <https://doi.org/10.1155/2012/427453>
3. U.I. Gaya, A.H. Abdullah, Heterogeneous photocatalytic degradation of organic contaminants over titanium dioxide: a review of fundamentals, progress and problems. *J. Photochem. Photobiol. C* **9**(1), 1–12 (2008)
4. R.W. Matthews, Photocatalytic oxidation of organic contaminants in water: an aid to an environmental preservation. *Pure Appl Chem.* **64**, 1285–1290 (1992)
5. Y. Wang, Y. Hao, H. Cheng et al., Photoelectrochemistry of transition metal-ion-doped TiO₂ nanocrystalline electrodes and higher solar cell conversion efficiency based on Zn²⁺-doped TiO₂ electrode. *J. Mater. Sci.* **34**(12), 2773–2779 (1999)
6. N. Venkatachalam, M. Palanichamy, V. Murugesan, Sol-gel preparation and characterization of nanosize TiO₂: its photocatalytic performance. *Mater. Chem. Phys.* **104**(2–3), 454–459 (2007)
7. T.B. Nguyen, M.J. Hwang, K.S. Ryu, Synthesis and high photocatalytic activity of Zn-doped TiO₂ nanoparticles by sol-gel and ammonia-evaporation method. *Bull. Korean Chem. Soc.* **33**(1), 243 (2012)
8. Y.N. Li, J. Su, X.Y. Lv, Y.F. Long, H. Yu, R.R. Huang, Y.C. Xie, Y.X. Wen, Zn²⁺-doped TiO₂/C with enhanced sodium-ion storage properties. *Ceram. Int.* (2017). <https://doi.org/10.1016/j.ceramint.2017.05.063>
9. D.S. Yao, Y.L. Zhao, L. Zhu, J. Song, X.Q. Gu, J.J. Zhu, Y.H. Qiang, Preparation of zinc-doped titanium dioxide nanorod arrays and their application in dye sensitized solar cells. *Int. J. Electrochem. Sci.* **10**, 5914–5923 (2015)
10. G. Liu, X. Zhang, Y. Xu, X. Niu, L. Zheng, X. Ding, The preparation of Zn²⁺-doped TiO₂ nanoparticles by sol-gel and

- solid phase reaction methods respectively and their photocatalytic activities. *Chemosphere* **59**, 1367–1371 (2005)
11. M. Qiao, S. Wu, Q. Chen, J. Shen, Novel triethanolamine assisted sol–gel synthesis of N-doped TiO₂ hollow spheres. *Mater. Lett.* **64**(12), 1398–1400 (2010)
 12. J.C.S. Wu, C.H. Chen, A visible-light response vanadium-doped titania nanocatalyst by sol–gel method. *J. Photochem. Photobiol. A* **163**(3), 509–515 (2004)
 13. J. Yang, X. Zhang, C. Wang, Solar photocatalytic activities of porous Nb-doped TiO₂ microspheres prepared by ultrasonic spray pyrolysis. *Solid State Sci.* **14**, 139–144 (2012)
 14. P. Bharathi, S. Harish, J. Archana, M. Navaneethan, S. Pon-nusamy, C. Muthamizhchelvan, M. Shimomura, Y. Haya-kawa, Enhanced charge transfer and separation of hierarchical CuO/ZnO composites: the synergistic effect of photocatalysis for the mineralization of organic pollutant in water. *Appl. Surf. Sci.* **484**, 884–891 (2019)
 15. C.H. Nguyen, C.C. Fu, R.S. Juang, Degradation of methylene blue and methyl orange by palladium-doped TiO₂ photo-catalysis for water reuse: efficiency and degradation path-ways. *J. Clean. Prod.* (2018). <https://doi.org/10.1016/j.jclepro.2018.08.110>
 16. R. Nainani, P. Thakur, M. Chaskar, Synthesis of silver doped TiO₂ nanoparticles for the improved photocatalytic degrada-tion of methyl orange. *J. Mater. Sci. Eng. B* **2**(1), 52–58 (2012)
 17. R.R. Bhosale, S.R. Pujari, G.G. Muley, S.H. Patil, K.R. Patil, M.F. Shaikh, A.B. Gambhire, Solar photocatalytic degrada-tion of methylene blue using doped TiO₂ nanoparticles. *Sol. Energy* **103**, 473–479 (2014)
 18. M.R.D. Khaki, M.S. Shafeeyan, A.A.A. Raman, W.M.A.W. Daud, Evaluating the efficiency of nanosized Cu doped TiO₂/ZnO photocatalyst under visible light irradiation. *J. Mol. Liq.* **258**, 354–365 (2017)
 19. P. Benjwal, K.K. Kar, Removal of methylene blue from waste water under a low power irradiation source by Zn, Mn co-doped TiO₂ photocatalysts. *RSC Adv.* **5**, 98166–98176 (2015)
 20. H.J. Seo, J.H. Boo, H.W. Jang, M.J. Kim, J.H. Boo, Photo-catalytic activity enhancement of TiO₂ with adding Zn par-ticles. *App. Sci. Converg. Technol.* **25**(6), 162–165 (2016)
 21. K. Jiang, J. Zhang, R. Luo, Y. Wan, Z. Liu, J. Chen, A facile synthesis of Zn-doped TiO₂ nanoparticles with highly exposed (001) facets for enhanced photocatalytic perfor-mance. *RSC Adv.* **11**, 7627 (2021)
 22. T. Rajaramanan, S. Shanmugaratnam, V. Gurunathanan, S. Yohi, D. Velauthapillai, P. Ravirajan, M. Senthilnathanan, Cost effective solvothermal method to synthesize Zn-doped TiO₂ nanomaterials for photovoltaic and photocatalytic degradation applications. *Catalysts* **11**, 690 (2021)
 23. J.J. Li, S.C. Cai, Z. Xu, X. Chen, J. Chen, H.P. Jia, J. Chen, Solvothermal syntheses of Bi and Zn co-doped TiO₂ with enhanced electron-hole separation and efficient photodegra-dation of gaseous toluene under visible-light. *J. Hazard. Mater.* **325**, 261–270 (2017)
 24. D. Gupta, R. Chauhan, N. Kumar, V. Singh, V.C. Srivastava, P. Mohanty, T.K. Mandal, Enhancing photocatalytic degrada-tion of quinoline by ZnO:TiO₂ mixed oxide: optimization of operating parameters and mechanistic study. *J. Environ. Manag.* **258**, 110032 (2020)
 25. J. Zhang, D. Fu, S. Wang, R. Hao, Y. Xie, Photocatalytic removal of chromium(VI) and sulfite using transition metal (Cu, Fe, Zn) doped TiO₂ driven by visible light: feasibility, mechanism and kinetics. *J. Ind. Eng. Chem.* (2019). <https://doi.org/10.1016/j.jiec.2019.07.027>
 26. M.K. Yeo, M. Kang, The effect of nano-scale Zn-doped TiO₂ and pure TiO₂ particles on Hydra magnipapillata. *Mol. Cell Toxicol.* **6**, 9–17 (2010)
 27. J. Yu, C. Gong, Z. Wu, Y. Wu, W. Xiao, Y. Su, L. Sun, C. Lin, Efficient visible light induced photoelectrocatalytic hydrogen production using CdS sensitized TiO₂ nanorods on TiO₂ nanotube arrays. *J. Mater. Chem. A* **3**, 22218–22226 (2015)
 28. M.P.B. Vega, J.L.G. Mar, M.V. Rodriguez, L.M. Trevino, L.L.G. Tovar, A.H. Ramirez, L.H. Reyes, Photocatalytic elimination of biphenol A under visible light using Ni-doped TiO₂ synthesized by microwave assisted sol-gel method. *Mater. Sci. Semicond. Process.* **71**, 275–282 (2017)
 29. M. Ahamed, M.A. Majeed Khan, M.J. Akhtar, H.A. Alhad-laq, A. Alshamsan, Role of Zn dopin in oxidative stress mediated cytotoxicity of TiO₂ nanoparticles in human breast cancer MCF-7 cells. *Sci. Rep.* **6**, 30196 (2016)
 30. I. Elmehasseb, S. Kandil, K. Elgendy, Advanced visible light applications utilizing modified Zn doped TiO₂ nanoparticles via non-metal in situ dual doping for wastewater detoxifica-tion. *Optik* **213**, 164654 (2020)
 31. Y. Yu, J. Wang, W. Li, W. Zheng, Y. Cao, Doping mechanism of Zn²⁺ ions in Zn-doped TiO₂ prepared by a sol–gel method. *CrystEngComm* **17**, 5074–5080 (2015)
 32. R.G. Nair, S. Mazumdar, B. Modak, R. Bapat, P. Ayyub, K. Bhattacharyy, The role of surface O-vacancies in the photo-catalytic oxidation of methylene blue by Zn-doped TiO₂: a mechanistic approach. *J. Photochem. Photobiol. A Chem.* **345**, 36–53 (2016)
 33. V.R. Akshay, B. Arun, G. Mandal, M. Vasundhara, Structural, optical and magnetic behavior of sol–gel derived Ni-doped dilute magnetic semiconductor TiO₂ nanocrystals for advanced functional applications. *Phys. Chem. Chem. Phys.* **21**, 2519–2532 (2019)

34. H.C. Choi, Y.M. Jung, S.B. Kim, Size effects in the Raman spectra of TiO₂ nanoparticles. *Vib. Spectrosc.* **37**, 33–38 (2005)
35. T. Ohsaka, E. Izumi, Y. Fujiki, Raman spectra of anatase TiO₂. *J. Raman Spectrosc.* **7**, 321–324 (1978)
36. T.T. Loan, V.H. Huong, V.T. Tham, N.N. Long, Effect of zinc doping on the band gap and photoluminescence of Zn²⁺ doped TiO₂ nanowires. *Physica B* **532**, 210–215 (2017)
37. S. Prabakaran, K.D. Nisha, S. Harish, J. Archana, M. Navaneethan, S. Ponnusamy, C. Muthamizhchelvan, H. Ikeda, Y. Hayakawa, Synergistic effect of SnO₂ and ZnO in enhancing the electrical and optical properties of Anatase TiO₂. *Appl. Surf. Sci.* **498**(1), 143702 (2019)
38. M.S. Dominguez, G.M. Mendoza, M.J.R. Vargas, C.C.I. Malo, A.A.R. Rodriguez, A.V.A. Gonzalez, S.A.P. Garcia, R. Gomez, Synthesis of zn doped TiO₂ nanoparticles by the novel oil-in-water microemulsion method and their use for the photocatalytic degradation of phenol. *J. Environ. Chem. Eng.* **3**(4), 3037–3047 (2015)
39. R. Vershney, K. Chelaramani, A. Bhardwaj, N. Siddiqui, S.K. Verma, synthesis, photocatalytic and antibacterial activities of nickel doped TiO₂ nanoparticles. *Orient. J. Chem.* **34**(6), 2867–2871 (2018)
40. P.C.S. Bezerra, R.P. Cavaicante, A. Garcia, H. Wender, M.A.U. Martinez, G.A. Casagrande, J. Gimenez, P. Marco, S.C. Oliveira, A. Machulek, Synthesis, characterization and photocatalytic activity of pure and N-, B-, or Ag-doped TiO. *J. Braz. Chem. Soc.* **28**(9), 1788–1802 (2017)
41. K. Singh, S. Harish, A. Periyanyaga Kristy, V. Shivani, J. Archana, M. Navaneethan, M. Shimomura, Y. Hayakawa, Erbium doped TiO₂ interconnected mesoporous spheres as an efficient visible light catalyst for photocatalytic applications. *Appl. Surf. Sci.* **449**, 755–763 (2018)
42. H. Zhao, S. Cui, G. Li, N. Li, X. Li, 1T- and 2H-mixed phase MoS₂ nanosheets coated on hollow mesoporous TiO₂ nanospheres with enhanced photocatalytic activity. *J. Colloid. Interfaces Sci.* **567**, 10–17 (2020)
43. M.S. Al-Johani, Y.S. Al-Zaghayer, S.I. Al-Mayman, TiO₂/ZnO photocatalytic activity for hydrogen production. *Int. Sci. J. Environ. Sci.* (2015). <https://doi.org/10.13140/RG.2.1.3673.8640>
44. H. Seema, K.C. Kemp, V. Chandra, K.S. Kim, Graphene–SnO₂ composites for highly efficient photocatalytic degradation of methylene blue under sunlight. *Nanotechnology* **23**, 355705 (2012)
45. S.J. Mofokeng, V. Kumar, R.E. Kroon, O.M. Ntwaeaborwa, Structure and optical properties of Dy³⁺ activated sol-gel ZnO–TiO₂ nanocomposites. *J. Alloys Compd.* **711**, 121–131 (2017)
46. P. Singla, O.P. Pandey, K. Singh, Enhanced photocatalytic degradation of diethyl phthalate using Zn doped rutile TiO₂. *Indian J. Pure Appl. Phys.* **55**, 710–715 (2017)
47. S.E. Sherbiny, F. Morsy, M. Samir, O.A. Fouad, Synthesis, characterization and application of TiO₂ nanopowders as special paper coating pigment. *Appl. Nanosci.* **4**, 305–313 (2014)
48. M.K. Tariq, A. Riaz, R. Khan, A. Wajid, H. Haq, S. Javed, M.A. Akram, M. Islam, Comparative study of Ag, Sn or Zn doped TiO₂ thin films for photocatalytic degradation of methylene blue and methyl orange. *Mater. Res. Express* **6**, 106435 (2019)
49. F. Abbas, R. Bensaha, H. Tarore, The influence of Zn²⁺ doping and annealing temperature on grown-up of nanostructures TiO₂ thin films prepared by sol-gel dip-coating method and their photocatalytic application. *Optik* (2018). <https://doi.org/10.1016/j.ijleo.2018.11.020>
50. V.R. Akshay, B. Arun, S. Dash, A.K. Patra, G. Mandal, G.R. Mutta, A. Chanda, M. Vasundhara, Defect mediated mechanism in undoped, Cu and Zn-doped TiO₂ nanocrystals for tailoring the band gap and magnetic properties. *RSC Adv.* **8**, 41994 (2018)
51. N. Kumaresan, M.M.A. Sinthiya, K. Ramamurthi, R. Ramesh Babu, K. Sethuraman, Visible light driven photocatalytic activity of ZnO/CuO nanocomposites coupled with rGO heterostructures synthesized by solid-state method for RhB dye degradation. *Arab. J. Chem.* **13**(2), 3910–3928 (2019)
52. J. Archana, M. Navaneethan, Y. Hayakawa, Hydrothermal growth of monodispersed rutile TiO₂ nanorods and functional properties. *Mater. Lett.* **98**, 38–41 (2013)
53. J.D. Chen, W.S. Liao, Y. Jiang, D. Yu, M. Zou, H. Zhu, M. Zhang, M. Du, Facile fabrication of ZnO/TiO₂ heterogeneous nanofibres and their photocatalytic behaviour and mechanism towards rhodamine B. *Nanomater. Nanotechnol.* **6**, 9 (2016). <https://doi.org/10.5772/62291>
54. Y. Chen, H. Ding, S. Sun, Preparation and characterization of ZnO nanoparticles supported on amorphous SiO₂. *Nanomaterials* **7**, 217 (2017)
55. B.B. Çırak, B. Caglar, T. Kılınc, S.M. Karadeniz, Y. Erdogan, S. Kılıc, E. Kahveci, A.E. Ekinici, C. Çırak, Synthesis and characterization of ZnO nanorice decorated TiO₂ nanotubes for enhanced photocatalytic activity. *Mater. Res. Bull.* **109**, 160–167 (2018)
56. Z. Ali, S.N. Cha, J.I. Sohn, I. Shakir, C. Yan, J.M. Kim, D.J. Kang, Design and evaluation of novel Zn doped mesoporous TiO₂ based anodematerial for advanced lithium ion batteries. *J. Mater. Chem.* **22**, 17625 (2012)
57. K.S. Stefańska, A. Kubiaka, A. Piasecki, J. Goscińska, G. Nowaczyk, S. Jurga, T. Jesionowski, TiO₂–ZnO binary oxide

- systems: comprehensive characterization and tests of photocatalytic activity. *Materials* **11**, 841 (2018)
58. L. Lin, Y. Yang, L. Men, X. Wang, D. He, Y. Chai, B. Zhao, S. Ghoshroy, Q. Tang. A highly efficient TiO₂@ZnO n–p–n heterojunction nanorod photocatalyst. *Nanoscale* **5**, 588–593 (2013)
59. S. Harish, M. Sabarinathan, A. Periyanyaga Kristy, J. Archana, M. Navaneethan, H. Ikeda, Y. Hayakawa, ZnS quantum dots impregnated-mesoporous TiO₂ nanospheres for enhanced visible light induced photocatalytic application. *RSC Adv.* **7**, 26446–26457 (2017)
60. M.R.D. Khaki, M.S. Shafeeyan, A.A.A. Raman, W.M.A.W. Daud, Evaluating the efficiency of nano-sized Cu doped TiO₂/ZnO photocatalyst under visible light irradiation. *J. Mol. Liq.* **258**, 354–365 (2018)
61. P. Zhang, C. Shao, X. Li, M. Zhang, X. Zhang, Y. Sun, Y. Liu, In situ assembly of well-dispersed Au nanoparticles on TiO₂/ZnO nanofibers: a three-way synergistic heterostructure with enhanced photocatalytic activity. *J. Hazard. Mater.* **237–238**, 331–338 (2012)
62. B. Pant, H.R. Pant, N.A.M. Barakat, M. Park, K. Jeon, Y. Choi et al., Carbon nanofibers decorated with binary semiconductor (TiO₂/ZnO) nanocomposites for the effective removal of organic pollutants and the enhancement of antibacterial activities. *Ceram. Int.* **39**, 7029–7035 (2013)
63. H.R. Pant, C.H. Park, B. Pant, L.D. Tijing, H.Y. Kim, C.S. Kim, Synthesis, characterization, and photocatalytic properties of ZnO nano-flower containing TiO₂ NPs. *Ceram. Int.* **38**, 2943–2950 (2012)
64. Z. Huimin, C. Yue, Q. Xie, R. Xiuli, Preparation of Zn-doped TiO₂ nanotubes electrode and its application in pentachlorophenol photoelectrocatalytic degradation. *Chin. Sci. Bull.* **52**(11), 1456–1461 (2007)

Publisher's Note Springer Nature remains neutral with regard to jurisdictional claims in published maps and institutional affiliations.